SWELTO FluxGate Magnetometer: Installation and First Measurements

G. Capobianco[a1], G. Bergamin[b1], and A. Bemporad[c1]

[1] *INAF-Turin Astrophysical Observatory, via Osservatorio 20, 10025, Pino Torinese (TO), Italy.*

[a] e-mail: gerardo.capobianco@inaf.it
[b] e-mail: giorgio.bergamin@inaf.it
[c] e-mail: alessandro.bemporad@inaf.it

Abstract

In the framework of the project SWELTO - *Space WEather Laboratory in Turin Observatory*, a fluxgate magnetometer has been procured, tested and characterized, and then installed and optimized in the INAF - Turin Astrophysical Observatory. This instrument aims to detect local geomagnetic disturbances associated with major global storms, providing a local value of the so-called Dst (i.e., Disturbance Storm Time) index. The measurements reported here and acquired during the first months after installation show a very good agreement with other similar instruments acquiring data in the surroundings, and also a good agreement with the official Dst-index provided by the World Data Center (WDC) for Geomagnetism, Kyoto.

Keywords: Space Weather – Automated Tools – Forecasting – Geomagnetism – Ionospheric Disturbances – Dst index –Solar Storms – Magnetometer

1 Introduction

In the field of the Space Weather it is very important to have available measurements of the disturbances in the Earth's magnetic field (the geomagnetic field) that are generally generated by additional currents induced in the ionosphere or magnetosphere during a geomagnetic storm. At the Italian national level, these kinds of measurements are currently acquired by a few stations managed by the INGV (National Institute of Geophysics and Volcanology) and located in Castello Tesino (TN), L'Aquila (AQ), Duronia (CB), and Lampedusa (AG). INGV also manages geomagnetic observatories in Antarctica [*]. These data are also standardized and used to contribute to the global network of geomagnetic observatories called INTERMAGNET[†] (International Real-time Magnetic Observatory Network). The provision of data to INTERMAGNET requires standard specifications for measuring and recording equipment, and operating the observatories according to these standards requires considerable resources.

Considering the low geomagnetic latitudes at which the national observatories providing the measurements are located, the geomagnetic disturbances measured from Italy are generally associated with the intensification of the so-called magnetospheric ring currents, which flow in the innermost part of the Earth's magnetosphere in the opposite direction to the rotation of the planet and in the proximity of the magnetic equator. These currents, present even in the absence of a disturbance, are particularly intensified during a geomagnetic storm, producing an additional component of the magnetic field directed towards the south which is typically quantified in terms of the so-called "Dst-index". The measurement of the Dst-index provides an indirect estimate of the intensity of these currents and therefore of the geomagnetic storm. The worldwide reference institute for this measurement is the WDC[‡] (World Data Center) for Geomagnetism in Kyoto, Japan.

*. The list and coordinates of the INGV geomagnetic facilities is available at: https://roma2.ingv.it/index.php/infrastrutture-di-ricerca/osservatori/osservatori-geomagnetici (link verified on 11 Jan. 2025)
†. https://intermagnet.org/ (link verified on 11 Jan. 2025)
‡. https://wdc.kugi.kyoto-u.ac.jp/index.html (link verified on 11 Jan. 2025)

In this framework, one of the main purposes of the SWELTO project is (Bemporad *et al.* 2020): *"To calibrate, test, and deploy new sensors (or employ already existing sensors) acquiring measurements to characterize possible geomagnetic, ionospheric and atmospheric disturbances, hence effects related with Space Weather events in the nearby Earth environment"*. For this reason, a geomagnetic station has been developed by the SWELTO team to monitor the impact on Earth of solar activity by measuring variations of the geomagnetic field (Bemporad *et al.* 2023). Having been developed independently, the aim of this station is not to provide data to the INTERMAGNET network in the future.

The main objective of this technical report is to describe in detail the station, the data acquisition, and the data reduction. Since the station is fully operational from November 20, 2024 the first measurements will be reported, as well as the validation of the data and a first detection of a geomagnetic storm. The last two sections of the report are dedicated to the calibration/maintenance plan and to future perspectives.

2 The OATo GeoMag Station

The GeoMag station is installed near the "Marcon dome" (GPS Coordinates: $45°02'27.18''N$, $7°45'50.58''E$; GPS Altitude: 665m) at the INAF - Astrophysical Observatory of Torino (hereafter OATo), see Figure 1.

The OATo GeoMag station is composed by:

- The 3-axis **fluxgate magnetometer**;
- The **Analog-to-Digital Converter** (ADC) converting the analog signals of the magnetometer to digital values;
- The **Power Module** cabinet, providing the power signals required by the magnetometer;
- The **Control Computer** acquiring and storing the digital data provided by the ADC.

The main elements of the station are detailed in Table 1.

Item	Model	S/N
Magnetometer	Bartington Instrument Mag-13MS60	614
ADC	Measurement Computing USB-2404-10	1EA31D5
Power Supply 1	RS PRO IS70-12	—-
Power Supply 2	RS PRO IS70-12	—-
Shielded Cable	MULTICOMP PRO MP002367	—-

Table 1. Items of the OATo GeoMag station.

The magnetometer is installed in a 1.5 m deep shaft on the top of an aluminum tripod (i.e., non-ferromagnetic material) to facilitate his orientation. The shaft walls are in polyvinyl chloride (i.e., PVC) to avoid any magnetic interference. Pictures of the installation are shown in Figure 2. A sealing stopper is installed on the top of the shaft to avoid water infiltration inside, even if the magnetometer itself and the electrical connector are waterproof. Since the instrument will provide relative measurements, not absolute, a rough leveling of the magnetometer has been performed during the installation (accuracy: ±5 degrees). The Z-axis of the magnetometer has been oriented with an angle of 15 ± 5 degrees w.r.t. the magnetic north. The ADC, the Power Module, and the Control Computer are installed inside the dome.

A shielded 25m long cable provides the power to the magnetometer (i.e., +12Vdc, -12Vdc, and power ground) from the Power Module and transmits the analog signals from the magnetometer to the ADC. A functional block diagram of the entire system is shown in Figure 3.

The items of the station are described in details in the next paragraphs.

Figure 1. The location of the OATo GeoMag station (GPS Coordinates: $45°02'27.18''N$, $7°45'50.58''E$; GPS Altitude: 665m).

2.1 The magnetometer

Based on the NOAA Geomagnetic Field Calculator [§], the OATo GeoMag station will measure the three components of the geomagnetic field (from the World Magnetic Model, WMM) summarized in Table 2.

The station will be able to detect variations of the order of $\pm 0.5nT$ on each component of the magnetic field, which means, $12ppm$ for the vertical component (D-U), $22ppm$ for the N-S component, and $330ppm$ for the E-W component.

The selected magnetometer is a three-axis fluxgate magnetometer. The instrument specifications, extracted from the datasheet,[¶] are summarized in Table 3.

In addition to the magnetic field, the magnetometer provides in output also the measured temperature. As already mentioned before, the magnetometer has been installed with the Z-axis

§. https://www.ngdc.noaa.gov/geomag/calculators/magcalc.shtml#igrfwmm (link verified on 11 Jan. 2025)

¶. Datasheet available at: https://www.bartingtondownloads.com/wp-content/uploads/DS3143.pdf (link verified on 11 Jan. 2025)

Figure 2. Left: The "Marcon" dome with the magnetometer shaft. Right: The magnetometer inside the shaft and installed on the tripod.

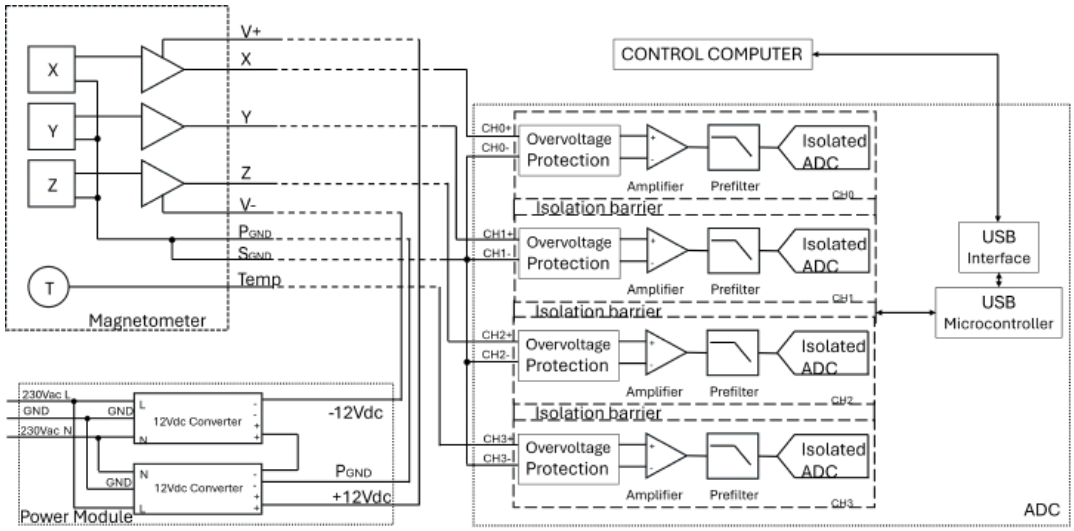

Figure 3. Functional block diagram of the OATo GeoMag station.

aligned with the direction N-S with an offset of 15 ± 5 degrees. The orientation of the magnetometer axes is reported in Table 4 and the reference system in Figure 4. The 25m long cable has been soldered to the connector following the scheme reported in Table 5. Details on how the fluxgate sensors work can be found in the bibliography (i.e, Gordon and Brown 1972).

Figure 4. The orientation of the magnetometer axes.

B component	Value [nT]	Drift [nT/year]
N-S	22817 ± 131	7.1
E-W	1510 ± 94	60.3
D-U	41889 ± 157	55.4

Table 2. Expected value of magnetic field for the OATo Geomag Station for the date of 20 November 2024.

Performance	Value
Full scale range	$\pm 60nT$
No. of axes	3
Scaling	$167mV/\mu T$
Scaling error	±0.5%
Linearity error	0.0015%
Noise	$< 10pT rms/\sqrt{(Hz)}$ @ 1Hz
Zero Field Offset	$< \pm 30nT$
Power Input	±12 to 17V
Analogue output	$\pm 10V$

Table 3. Performances of the fluxgate magnetometer.

2.2 The Analog-to-Digital Converter

The analog signals generated by the magnetometer are digitized by the analog-to-digital-converter (ADC). The main characteristics of the selected device, extracted from the instrument datasheet,‖ are summarized in Table 6.

The ADC is directly interfaced to the control computer through a USB 2.0 High-Speed interface that also provide the power to the device. The four channels of the ADC are simultaneously acquired. Since the input range of the ADC is of $\pm 10V$, corresponding to the analogue output voltage of the magnetometer, the 3+1 channels of the magnetometer are directly interfaced with the ADC. The scaling of the ADC is $S = \frac{20V}{2^{24}} = 1.192\frac{\mu V}{bit}$, corresponding to $7.1\frac{pT}{bit}$, the actual resolution of the instrument.

2.3 The Power Module

The magnetometer must be powered with $\pm 12V$, for that reason, two switching power supply connected in series are used (see the block diagram in Figure 3). The main characteristics of the power supply ** are summarized in Table 7.

The power module is electrically protected by a residual current circuit breaker and a circuit breaker. The output of the power supply are regulated by measuring the voltage at the terminals of the cable connected to the magnetometer. The measured voltage is $\pm 12.08V$.

An image of the power module is shown in Figure 5. The green LED indicates that the power supply is properly working.

2.4 The Control Computer

The control computer must have the interface listed in Table 8. The acquisition software is based on NI LabView. The software is designed to run on single-board computers (SBC) like Raspberry

‖. Datasheet available at: https://files.digilent.com/datasheets/USB-2404-series-data.pdf?_gl=1*1gihvj5*_gcl_au*MTM3NDQwODQ4NC4xNzMwMjE2NTk3*_ga*MjYxMjI1ODQ1LjE3MzAyMTY1OTc.*_ga_JSPEFFCPBT*MTczNTgyMzE2MS40LjAuMTczNTgyMzE2OC41My4wLjA.datasheet (link verified on 12 Jan. 2025)

**. Datasheet available at: https://docs.rs-online.com/4cfe/A700000007349990.pdf (link verified on 12 Jan. 2025)

Magnetometer axis	Orientation
X	E-W
Y	D-U
Z	N-S

Table 4. Orientation of the 3 axes of the magnetometer. An offset of 15 ± 5 degrees on the horizontal plane has been introduced.

Connector Pin Number	Function	Cable color
1	X+	Black
2	Y+	Yellow
3	Z+	Blue
4	PGND	White
5	SGND	Red
6	V+	Green
7	V-	Purple
8	Temp	Brown

Table 5. Summary of the electrical connection of the magnetometer.

Figure 5. Image of the power module.

and requires about 500 kB. The daily data amount depends on the acquisition settings and is at maximum 13 $\frac{MB}{day}$ if the data are stored every second. With the current acquisition rate, the software produces 2 files of 1.3 MB each per day.

A desktop computer installed inside the "Marcon" dome is used for the acquisition. On the control computer, only the data acquisition software is running. The data analysis pipeline runs on a different computer making plots and data available in real-time on the SWELTO webpage[††].

††. At this moment the real-time data display of these measurements is not yet available. See Par. 8. The SWELTO webpage is on-line at the web address: https://swelto.oato.inaf.it/ (link verified on 12 Jan. 2025)

Performance	Value
Number of Channels	4
Resolution	24-bit
Master Time-base Frequency (MTBF)	12.8 MHz
Sample rates	$f = \frac{MTBF/256}{n}, n = 1, 2, ...31$
Accuracy	better than $\pm 100 ppm$
Input voltage range (nominal)	$\pm 10V$
Input Noise	$70 \mu V rms$
Gain Error (calibrated)	±0.03%
Offset Error (calibrated)	±0.008%

Table 6. Performances of the Analog-to-Digital Converter extrapolated from the instrument datasheet.

Performance	Value
Number of power supply	2
Connection	Series
Type	Switch
AC Input Voltage	110-240 V_{AC}
DC Output Voltage	11-14 V_{DC}
Output Current	5A
Efficiency	84%
Ripple and Noise	100 mV

Table 7. Performances of the Power Supply Module.

3 Data Acquisition

The acquisition parameters are configurable by software. The list of reconfigurable parameters is reported in Table 9.

The software is sampling the signals at the selected frequency for the selected time. The average value and the standard deviation are stored in a file named "*YYYY_MM_DD-MagnetometerRaw.csv*". The same data are filtered with a band-pass 3^{rd} order Butterworth filter (low cut-off frequency:0.05 Hz, high cut-off frequency: 50Hz). The average and standard deviation are stored in the file named "*YYYY_MM_DD-MagnetometerFiltered.csv*". The output files are standard CSV files. The structure of the files is in Table 10.

4 Data Reduction

The temperature monitor chain of the ADC (i.e., ADC Channel#4) is processed as in Figure 6. Only two operations are performed on the data:

1. Removal of the ADC offset;
2. Conversion from voltage to Celsius.

The ADC Offset is periodically calibrated, for the used value see Par. 5.1, for the calibration plan see Par.7. The offset and gain of the sensor are extrapolated from the datasheet and they have the values of: $T_{Off} = 3500mV$; $T_{Gain} = -10\frac{mV}{^\circ C}$.

The magnetic field values are obtained from raw values by applying the following steps (see Figure 7). The figure refers to a single chain and is the same for the three channels.

1. Removal of not valid data by checking the validity flag value;
2. Removal of the ADC offset for the 4 channels;
3. Unit conversion of the signals (i.e., from Volts to nT for the magnetic field channels and from

Interface	Purpose
USB 2.0 High speed	ADC power and data acquisition
Ethernet (RJ 45)	Data exchange

Table 8. Required interface on the control computer.

Parameter	Description	Default value
Physical Channels	The device and channels to be acquired	—
Sampling Frequency	The acquisition frequency in ksps (kilo samples per seconds)	1.613
Time to average	The exposure time in seconds	5

Table 9. The parameters of the acquisition.

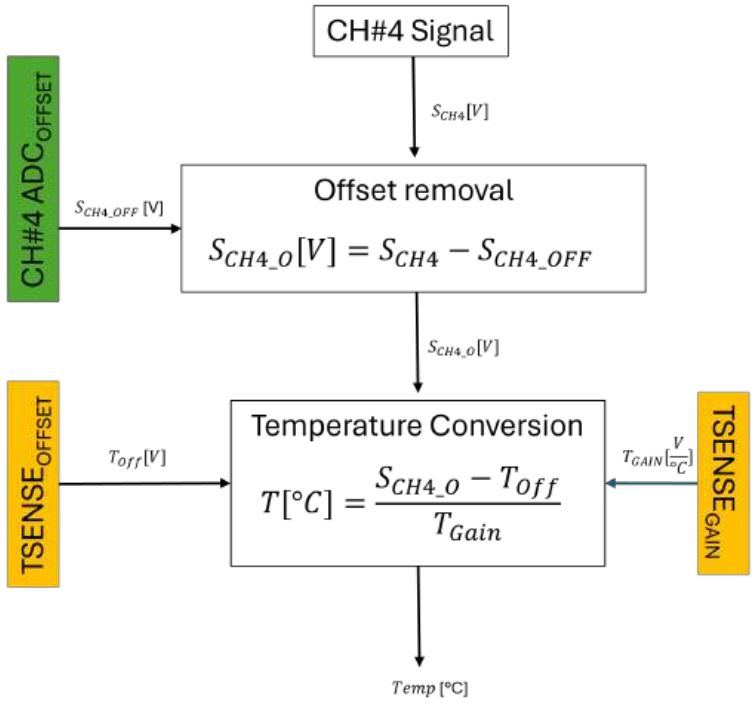

Figure 6. Temperature conversion flowchart.

Volts to Celsius for the temperature channel);

4. Correct the magnetic field measurements for the temperature.

At the moment, the temperature correction of the magnetic field measurements (i.e., step number 4) is not applied due to the uncertainties on the α_T parameter (more statistics in a wider temperature range is required). The ADC offset is periodically calibrated, for the used value see Par 5.1, for the calibration plan see Par. 7.

The ADC scale factor is defined as: $\beta = \frac{B_{range}}{V_{Range}} = \frac{120\mu T}{20V} = 6000[\frac{nT}{V}]$. The vertical component of the magnetic field corresponds to the B_Y component, $B_V \equiv B_Y$, when the horizontal component is $B_H = \sqrt{B_X^2 + B_Z^2}$.

4.1 Derivation of the Dst index

Starting from the measurements of the 3 components of the magnetic field (i.e., B_X,B_Y and B_Z) the first required step for the evaluation of the Disturbance Storm Time (Dst) index is the subtraction of

Column	Content	Units
1	Time	HH:MM:SS
2	Channel#1 Average	Volts
3	Channel#2 Average	Volts
4	Channel#3 Average	Volts
5	Channel#4 Average	Volts
6	Channel#1 Standard Deviation	Volts
7	Channel#2 Standard Deviation	Volts
8	Channel#3 Standard Deviation	Volts
9	Channel#4 Standard Deviation	Volts
10	Validity Flag	0 (not valid) or 1 (valid)

Table 10. Output file structure

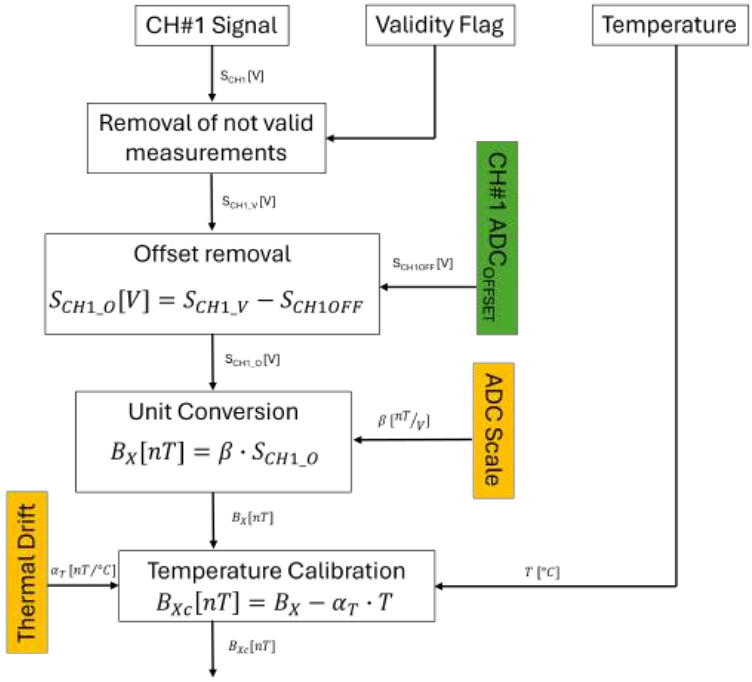

Figure 7. Magnetic Field calibration flowchart (for B_X component).

the relative unperturbed magnetic field (i.e, B_X^u, B_Y^u and B_Z^u) as reported in Eq. 1. The components of the unperturbed magnetic field at a certain time t_i are evaluated monthly by using the average value of the 5 international quietest days of the previous month. These days are the ones designed by the Helmholtz Centre for Geosciences[‡‡] in Potsdam, Germany.

$$\begin{cases} \Delta B_X(t_i) = B_X(t_i) - B_X^u(t_i) \\ \Delta B_Y(t_i) = B_Y(t_i) - B_Y^u(t_i) \\ \Delta B_Z(t_i) = B_Z(t_i) - B_Z^u(t_i) \end{cases} \quad (1)$$

The Dst index at the time t_i is then evaluated as the value of the component showing the highest variation in $\Delta B_{X,Y,Z}(t_i)$.

‡‡. https://kp.gfz-potsdam.de/en/data (link verified on 12 Jan. 2025)

Usually we provide the ΔB components every 5 minutes and the Dst index every hour, by using the maximum value of the Dst in the selected temporal range.

This calculation is a simplified procedure of the one described by (Sugiura and Kamei 1991). From The Dst index is possible to retrieve other indices commonly used for geomagnetic activity, solar-terrestrial physics, and space weather (Matzka *et al.* 2021; Menvielle and Marchaudon 2007).

5 First Data and Calibration

5.1 Calibration of the ADC offset

Before the installation at the "Marcon" Dome, a long-run data acquisition has been executed in the OATo laboratory in order to check the robustness of the data acquisition. This run lasted 130 days and was used to characterize the ADC offset since the magnetometer was not connected to the ADC. The results are shown in Figure 8 and summarized in Table 11. The data used for this evaluation refer to October 30, 2024. The ADC Offset calibration will be performed every 6 months (see Par. 7).

ADC Channel	Offset [mV]	RMS Error [mV]
1	0.0025	0.005
2	-0.865	0.005
3	-1.224	0.005
4	-1.668	0.005

Table 11. Measured offset of the 4 ADC channels (at room temperature).

5.2 First-month data and data validity evaluation

The magnetometer is fully operational since November 20, 2024. The data acquired during the first month, until December 23, 2024, are used to evaluate the performances and the validity of the data acquired by the station.

Warm-up time

The warm-up time of the magnetometer is expected to be about 2 hours. The measured temperature confirms this behavior as shown in Fig. 9. The acquisition started at 16:06:56 UTC and after 2 hours (i.e., at 18:07 UTC) the temperature was completely stabilized.

Effectiveness of the thermal insulation

One of the reasons for the installation of the magnetometer inside the shaft is the reduction of the thermal variations. In Fig. 10 the magnetometer temperature (average and max-min area) are shown together with the air temperature (average and max-min area)[§§]. The average of the daily variations for the magnetometer temperature is $0.6^{\circ}C$ while for the air is $9.4^{\circ}C$. From these results, we can conclude that from the thermal point of view, the use of a shaft is a good solution.

Magnetic field values

The validity of the geomagnetic data from the magnetometer is verified by comparing the acquired values with:

1. The expected value from the WMM model;
2. The values acquired by the Duronia (DUR) station.

§§. The temperature data are provisional data provided by a meteo station installed on the roof of the Observatory and managed by the ARPA Piemonte: https://www.arpa.piemonte.it/rischi_naturali/snippets_arpa_graphs/dati_giornalieri_meteo/?statid=PIE-001192-900-1988-05-19&param=T (link verified on 12/01/2024)

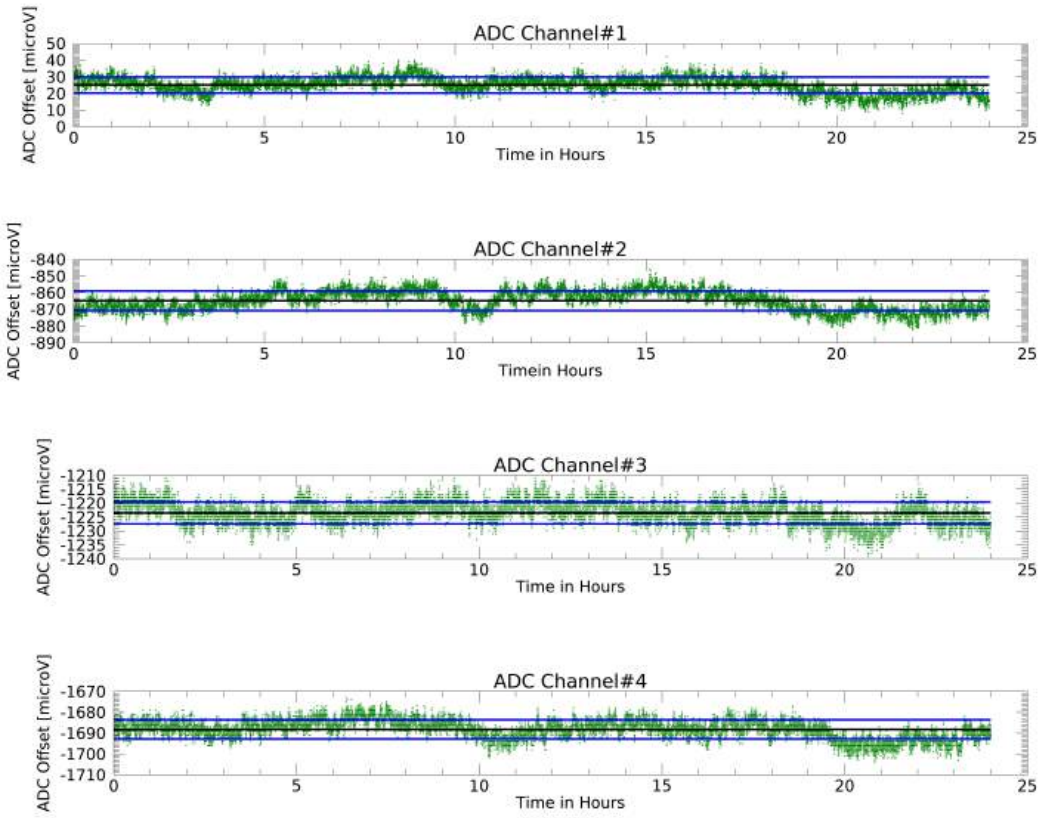

Figure 8. Measured offset of the 4 ADC channels. In green the data distribution and average (black) with the RMS value (blue) are over-plotted.

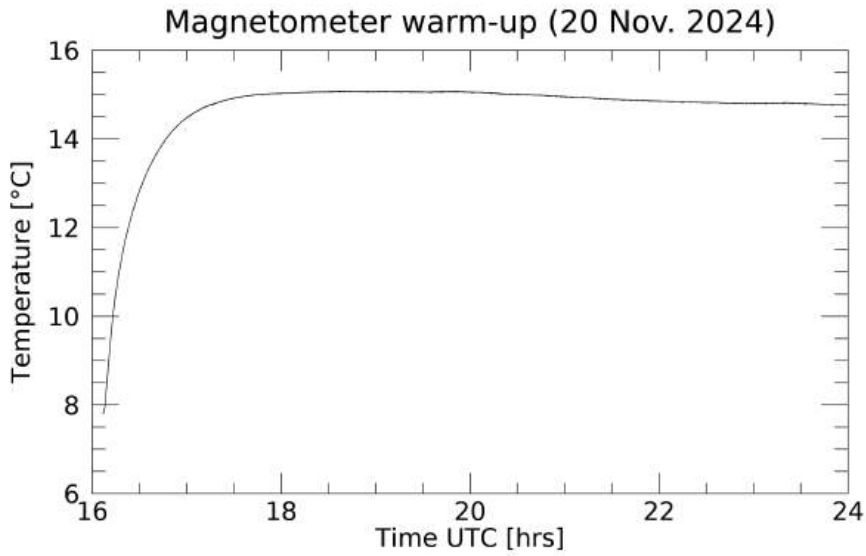

Figure 9. Warm-up of the magnetometer least around 2 hours as expected.

The data for the horizontal component, B_H, and the vertical component, B_V are in shown Figures 11 and 12.

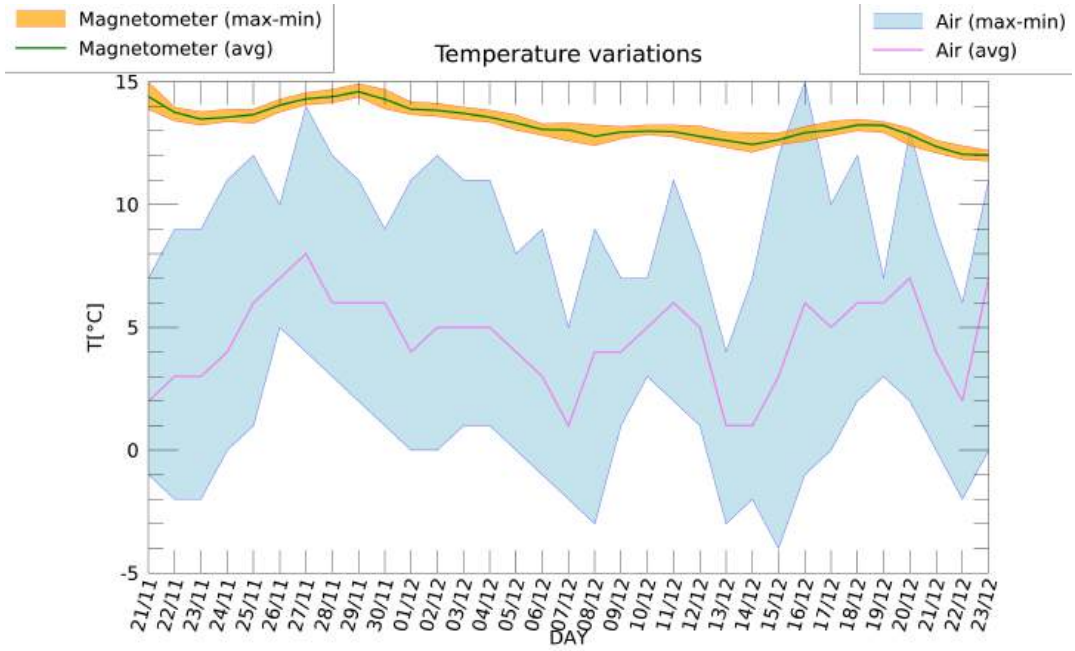

Figure 10. Temperature variations for the magnetometer and for the air for the dates from November 21, 2024 to December 23, 2024.

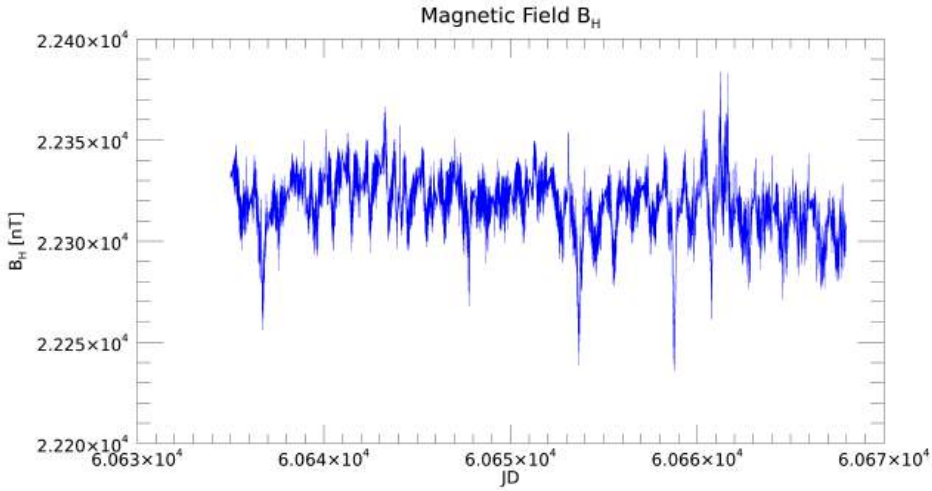

Figure 11. Horizontal component of the magnetic field B_H. Measurements from 21 Nov. 2024 00:00:00 UTC to 24 Dec. 2024 00:00:00 UTC.

The measurements average values are: $\overline{B_H} = 22319 \pm 14nT$ and $\overline{B_V} = 48010 \pm 8nT$. The horizontal component is affected by the declination of the site, expected to be $\delta_{site} = 3.16$ degrees, and by the offset introduced in the alignment (i.e., 15 ± 5 degrees). The check on the declination, obtained as a ratio between the measured $B_H^{(meas)}$ value and the expected one $B_H^{(exp)}$ is: $\delta = \arccos[\frac{B_H^{(meas)}}{B_H^{(exp)}}] = 13$ degrees. This result is inside the range we expect to measure. The inclination is by definition $I = \arctan[\frac{B_V}{B_H}]$. From the measurements we obtain $I = 65$ degrees. Since the expected value is 61.2 degrees, with an error of ± 5 degrees due to the alignment, we can conclude

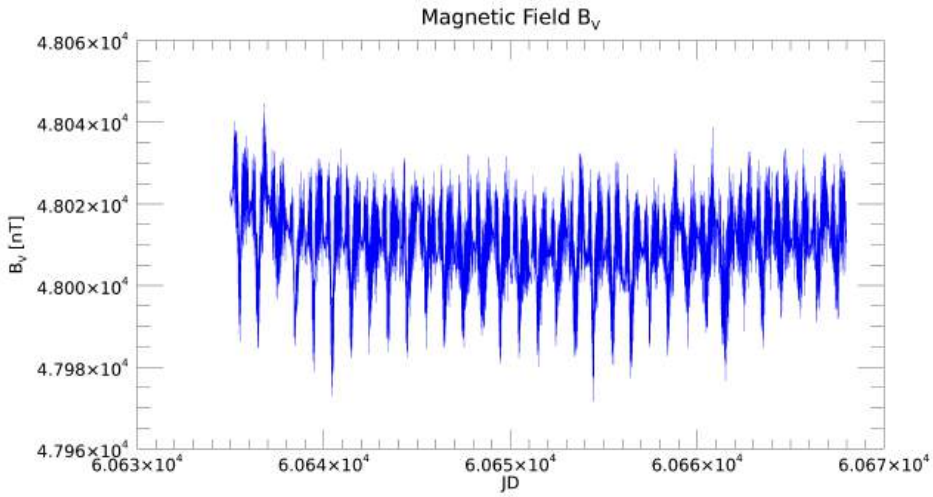

Figure 12. Vertical component of the magnetic field B_V. Measurements from 21 Nov. 2024 00:00:00 UTC to 24 Dec. 2024 00:00:00 UTC.

that the measurements are consistent with the expected values within the errors and the device is properly working.

By comparing theB_V and B_H data with the values of the Duronia station, as in Figure 13, it is clear that the magnetic field was disturbed during the period under examination, since both the plots show similar variation at the same time.

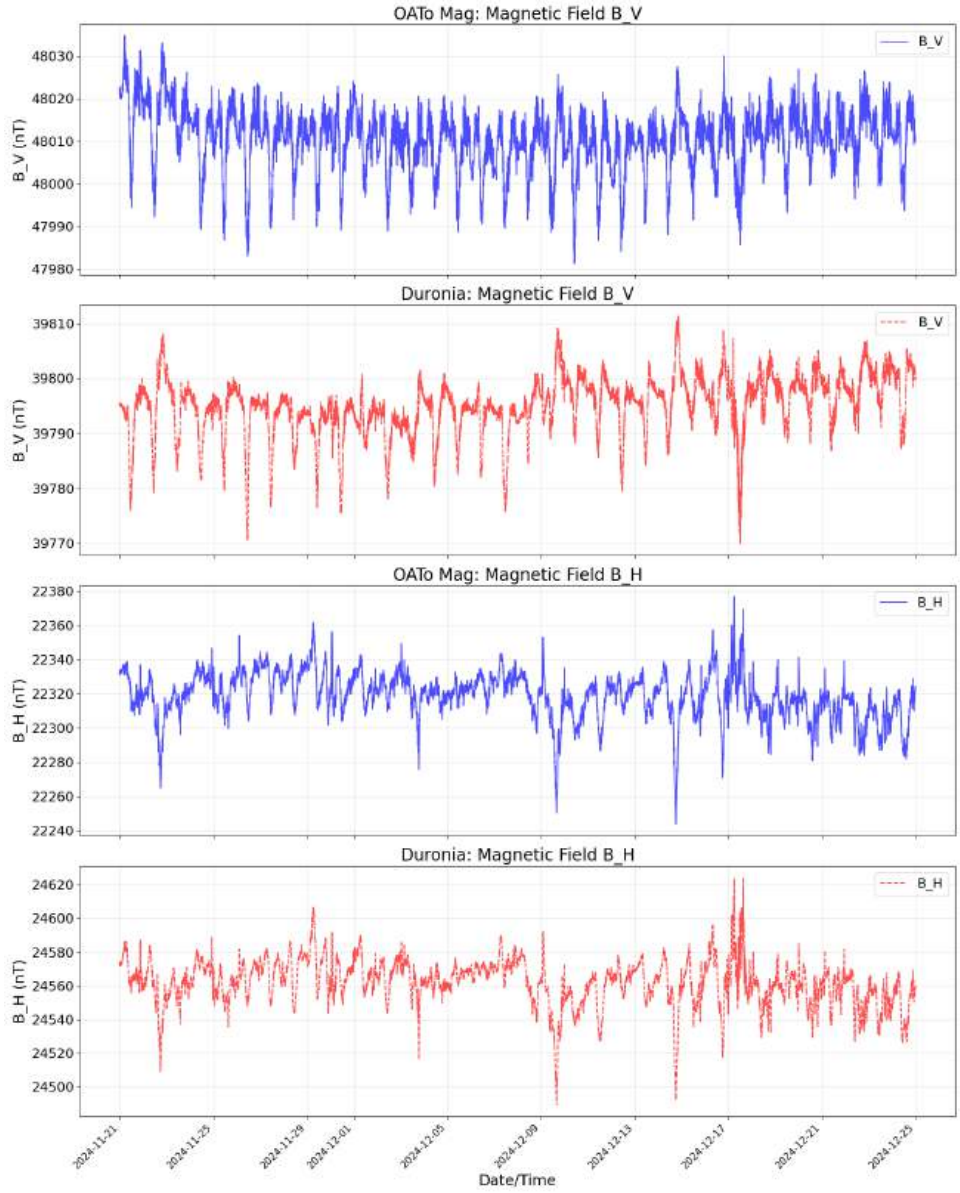

Figure 13. Data available for Duronia station compared with the OATo magnetic station. The top plots refers to B_V values (blue for OATo and red for Duronia). The botoom plots refers to B_H values (blue for OATo and red for Duronia).

From this comparison we can conclude that the big value of the standard deviation observed in the average values of the magnetic field measurements are due to real perturbations of the magnetic field as measured from both the stations.

Frequency analysis

A Fourier analysis has been performed on the acquired signals to check their periodicity. The power spectra of the three axes (see Figure 14 for the spectra for the B_Y axis, as an example) clearly show that the most significant periodic signal has a frequency of $1.157E-5$ Hz corresponding to a period of 24H.

Apart from the harmonics of the main frequency no more periodic signals are found on the spectra. This analysis also suggests that the signals from the magnetometer should be "cleaned"

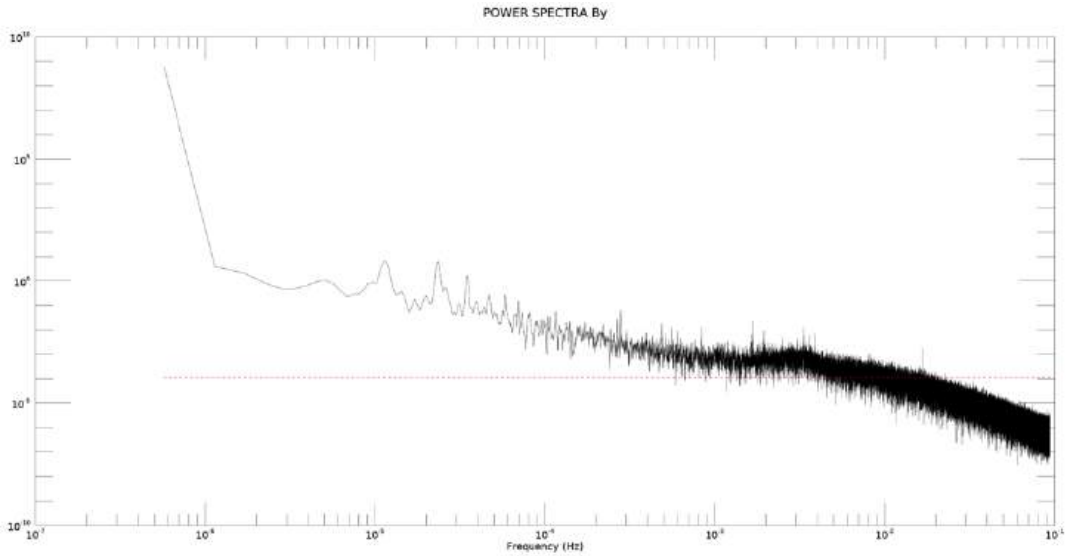

Figure 14. Power spectra of the B_Y signal. The 95% significance level is also represented by the red dotted line.

by removing the frequencies higher than 10^{-4} Hz.

Dst-index

By applying the procedure described in the Par. 4.1 from the raw data we can retrieve the Dst index for the days from November 21 to December 23. The retrieved un-perturbated magnetic field curve is shown in Fig. 15.

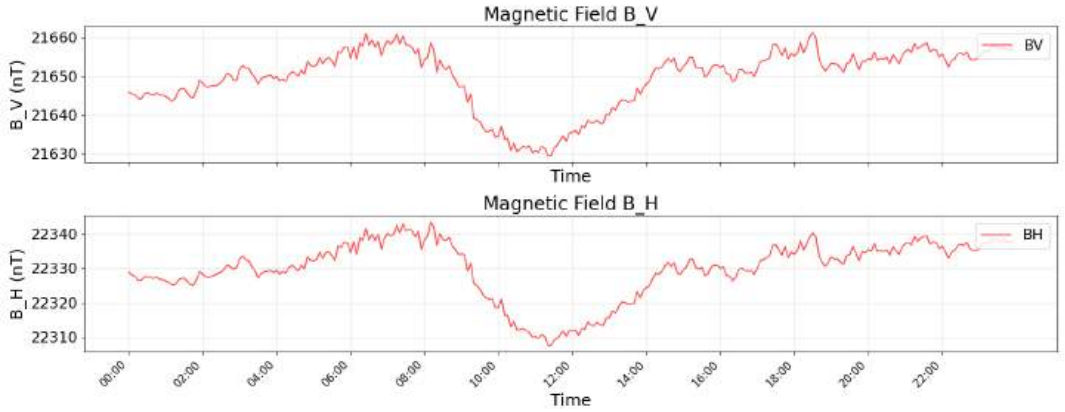

Figure 15. Un-perturbated B_V^u and B_H^u value of the OATo magnetic station.

The retrieved Dst- index, compared with the Kyoto Dst-index is shown in Fig. 16.

6 Detection of January 1st 2025 Geomagnetic Storm

The first measurements that were acquired since the end of November allowed us to obtain a preliminary local reference curve in undisturbed conditions, a curve that was then used to measure the disturbance induced daily in the local geomagnetic field, following a procedure similar to that described in (**Sugiura1991**). Solar events that occurred in early 2025 generated an unexpectedly intense G4-class geomagnetic storm on New Year's Day, leading to the formation of intense Auroras

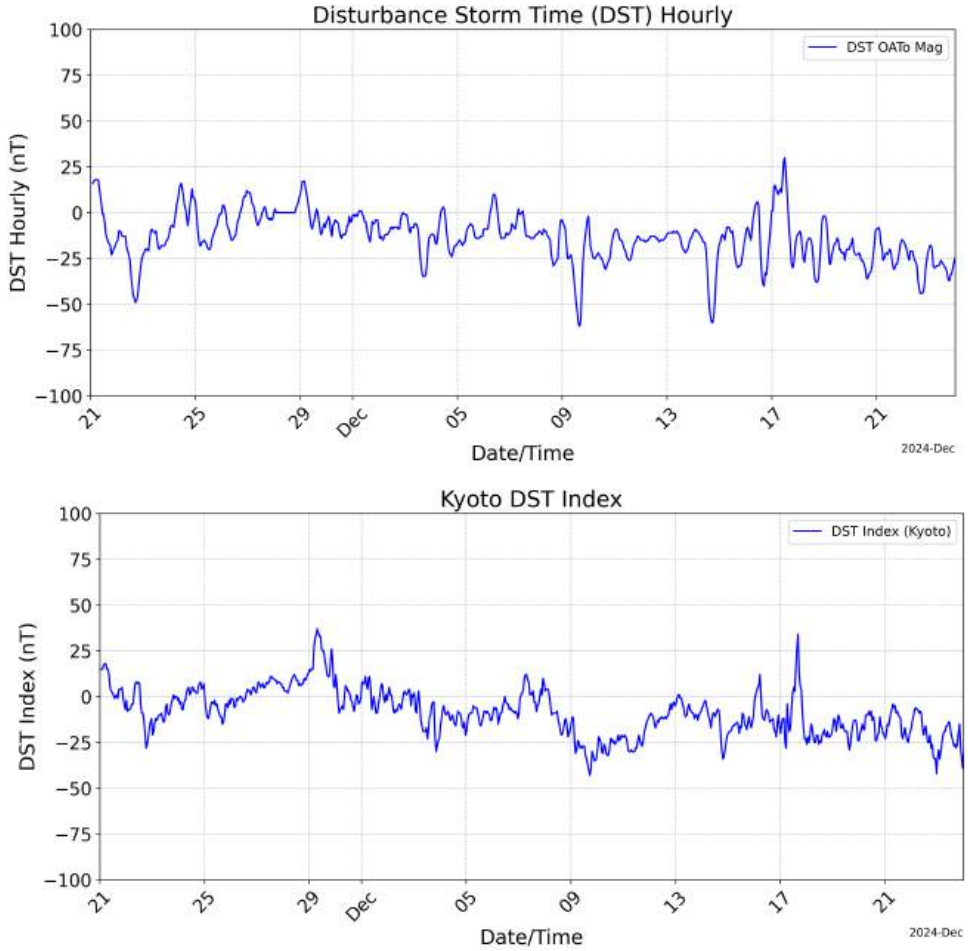

Figure 16. Comparison of DST index from the OATo station (top) and Kyoto (bottom).

also observed from Italy on the night between 1 and 2 January. This event represented a unique opportunity to verify the correct functioning of the new INAF magnetometer in Turin acquired as part of the Swelto project. Fig. 17

The data obtained from the Swelto magnetometer clearly show the local detection of the geomagnetic disturbance, with a minimum value of the local Dst-index equal to –277 nT at 17:25 Ut on January 1st, in excellent agreement with the official value equal to – 215 nT at 17 Ut of the same day. The curve obtained from the INAF sensor also correctly shows all the phases of the geomagnetic storm, both the phase of rapid decrease in the Dst index (called "main phase") and the subsequent phase of recovery of the initial value of the geomagnetic field (called "recovery phase"). Fig. 18

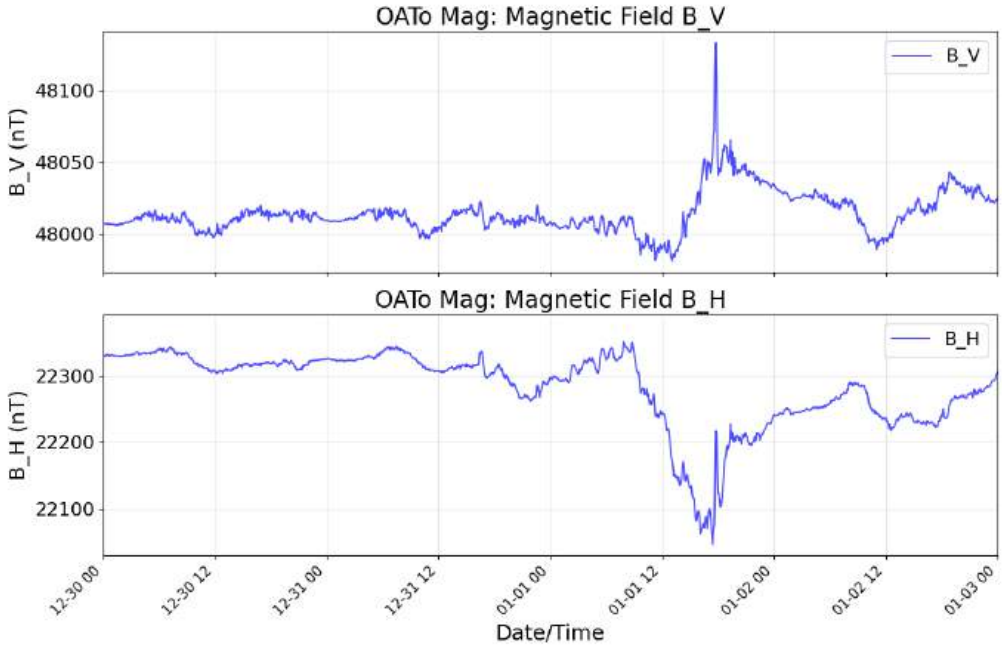

Figure 17. Magnetic field measurements from December 30, 2024 to January 3, 2025 of B_V (top) and B_H (bottom). A big change in the magnetic field is measured during the night between January 1^{st} and January 2^{nd}.

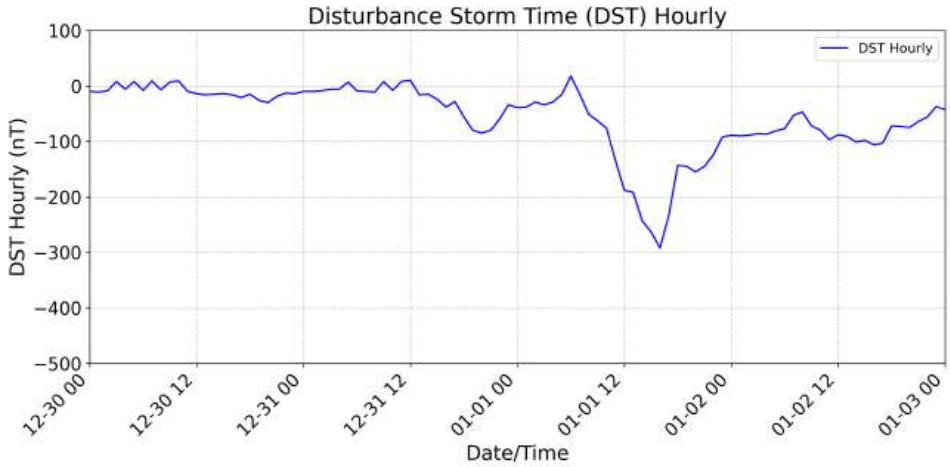

Figure 18. The DST index during the storm as retrieved from the OATo GeoMag station.

7 Calibration and maintenance plan

The periodic calibration of some parameters is required, in order to proper correct the data. In Table 12 are summarized the parameters to be calibrated and the period between calibrations.

8 Conclusions and future perspectives

As observed from the initial acquisition and calibration, the data is promising and reflects a disturbed magnetic field. Furthermore, note how the calculation of the IMF (difference between the disturbed EMF and the quiet sun curve) aligns with NASA's data.

The INAF SWELTO magnetometer is therefore already able to detect the occurrence of geomag-

Parameter	Calibration period	Next calibration
ADC Offset	every 6 months	May 2025
Voltage to magnetometer	every 6 months	May 2025
ADC range	every year	November 2025
ADC scale	every year	November 2025

Table 12. Periodically re-calibrated parameters.

netic storms locally in real-time. In the near future, we plan to publish the measurements in near real-time on the dedicated portal of the SWELTO project, where the latest data acquired in situ by the ACE probe in the L1 Lagrangian point and the latest measurements of the Dst-index provided by Kyoto are already shown.

At the moment an internet connection is not available inside the "Marcon" dome and this is the biggest stop to have data in real-time on the SWELTO webpage. We plan to have the computer online in the next few months.

Acknowledgments

The SWELTO project is entirely supported locally by the INAF-Turin Astrophysical Observatory, and by national funding received by INAF to support activities related with Space Weather discipline.

References

Bemporad, A., L. Abbo, D. Barghini, C. Benna, D. Biond R.and Bonino, G. Capobianco, F. Carella, *et al.* 2020. *SWELTO-Space WEather Laboratory in Turin Observatory.* INAF Technical Reports 40. Published on-line. INAF-Turin Astrophysical Observatory, via Osservatorio 20, 10025 Pino Torinese (TO), Italy: INAF, June.

Bemporad, A., S. Fineschi, L. Abbo, C. Benna, R. Biondo, G. Capobianco, F. Carella, *et al.* 2023. “Space weather-related activities and projects on-going at INAF-Turin Observatory.” *Rendiconti Lincei. Scienze Fisiche e Naturali* 34, no. 4 (December): 1055–1076. https://doi.org/10.1007/s12210-023-01193-x.

Gordon, D., and R. Brown. 1972. “Recent advances in fluxgate magnetometry.” *IEEE Transactions on Magnetics* 8, no. 1 (March): 76–82. https://doi.org/10.1109/TMAG.1972.1067268.

Matzka, J., C. Stolle, Y. Yamazaki, O. Bronkalla, and A. Morschhauser. 2021. “The Geomagnetic Kp Index and Derived Indices of Geomagnetic Activity.” *Space Weather* 19, no. 5 (May): e2020SW002641. https://doi.org/10.1029/2020SW002641.

Menvielle, M., and A. Marchaudon. 2007. “Geomagnetic Indices in Solar-Terrestrial Physics and Space Weather.” In *Space Weather : Research Towards Applications in Europe 2nd European Space Weather Week (ESWW2),* edited by J. Lilensten, 344:277. Astrophysics and Space Science Library. January. https://doi.org/10.1007/1-4020-5446-7_24.

Sugiura, M., and T. Kamei. 1991. *IAGA Bulletin No. 40, Equatorial Dst Index 1957-1986.* ISGI Pubblications Office. https://doi.org/10.25577/z1kh-9196.